Heliyon

ELSEVIER

Received:
20 October 2018
Revised:
24 November 2018
Accepted:
28 November 2018

Cite as: I. G. Shuttleworth. The quasiparticle band structures of ordered Ni_xPt_{1-x}. Heliyon 4 (2018) e01000. doi: 10.1016/j.heliyon.2018.e01000

The quasiparticle band structures of ordered Ni_xPt_{1-x}

I. G. Shuttleworth*

School of Science and Technology, Nottingham Trent University, Nottingham, NG11 8NS, UK

* Corresponding author.

E-mail address: ian.shuttleworth@ntu.ac.uk (I.G. Shuttleworth).

Abstract

The quasiparticle band structures of the ordered $L1_2$ and $L1_0$ phases of Ni_xPt_{1-x} ($x = 0.25$, 0.5, and 0.75) have been calculated and compared to the band structures obtained using density functional theory. For each alloy, an increase in the curvature of the band structure is generally seen when the quasiparticle correction is made. Non-dispersive regions are shown to include a dispersive component under the quasiparticle correction. The quasiparticle weights are k-dependent and greater towards the Γ point. Non-linear analytical modelling of the quasiparticle correction is shown to be complex.

Keywords: Materials science, Physical chemistry, Theoretical chemistry, Condensed matter physics, Quantum mechanics

1. Introduction

The ordered phases of ordered Ni_xPt_{1-x} ($x = 0.25$, 0.5, and 0.75) are transition metal alloys whose structural and electronic states depend sensitively on their stoichiometry and both the temperature and pressure of their surroundings [1]. At high temperatures (>600−800 K) the alloys are disordered but at lower temperatures ordered structures form [2, 3]. This phenomenology is also seen for the associated Co-Pt and Fe-Pt systems and the ordering reduces much of the structural complexity of the systems and allows them to be theoretically much more accessible.

https://doi.org/10.1016/j.heliyon.2018.e01000

Theoretical investigations of the electronic band structure have focussed on the disordered phases. Early studies by Staunton et al. [4] calculated the band structure along the Γ-X direction of the $Ni_{0.50}Pt_{0.50}$ alloy using the relativistic Korringa-Kohn_Rostocker coherent potential approximation (R KKR CPA). The work predicted only modest changes in the band structure with Pt or Ni concentration for the disordered case and was limited by the KKR treatment of the site potentials and their self-consistency. The prediction of DOS at the Fermi level was lower than the DOS observed experimentally [5]. The work was complemented by self-consistent field (SCF) KKR-CPA calculations [6, 7] of the $Ni_{0.50}Pt_{0.50}$ alloy which calculated the ordering and the alloy formation energy. Recent developments [8] have shown that the non-local coherent potential approximation (NL-CPA) is effective in describing the electronic structure of disordered alloys; however, no re-investigation of the electronic band structure of the disordered Ni-Pt alloy or investigation of the ordered Ni-Pt alloys have been presented. Combined experimental and computational studies [9] have concluded that relativistic and self-consistent effects are required within KKR-CPA calculations in order to explain the weight of Pt states close to the Fermi level which are seen in experimental photoemission studies of the disordered Ni-Pt and Cu-Pt alloys. Later studies [10] concluded that electron correlation was one of the more probable causes of discrepancies between computational and experimental studies of Ni-Pt alloys. These conclusions support the use of quasiparticle methods over conventional DFT approaches in computational studies of these alloys.

The work outlined in the previous paragraphs have highlighted the fundamental interest in both ordered and disordered Ni-Pt alloys. Significant applied interest exists for these systems particularly since the observation that the $Pt_3Ni(111)$ surface is significantly more reactive towards the oxygen reduction reaction (ORR) than pure Pt(111) [11,12]. These surfaces are made out of Pt overlayers lying on top of an alloy bulk which is phenomenon seen across a range of metallic alloys [13]. These surface layers are subject to both geometric and electronic effects. Geometrically the pure Pt surface layers are strained compared to the surface layers of Pt(111) which are formed above a pure Pt bulk. This is because the bulk alloy will have a different lattice constant to bulk Pt. The importance of the effects of strain on Pt(111) towards reactants in the ORR have recently been investigated [14, 15]. The electronic structure of the Pt(111) surface layer will be affected by the nature of the selvedge and, to a lesser extent, the bulk. This is because the wave-functions in these regions will interact with those in the surface. Recent computational studies have focussed on the selvedge character by applying strain to Ni-Pt [16], and both the Co-Pt and Fe-Pt systems [17] and have discussed the magnetic character of these alloys under both compressive and tensile loading.

In the current work the quasiparticle approximation will applied to the ordered Ni_xPt_{1-x} ($x = 0.25$, 0.5, and 0.75) alloys and will be compared with the predictions

https://doi.org/10.1016/j.heliyon.2018.e01000

of density functional theory (DFT). The work is organised in following way: in the Computational Details, the level of both quasiparticle and DFT approximation used in the current work is outlined together with a complete description of the metrics used to compare both of these approaches as well as a short summary of their geometric and magnetic predictions. The Results and Discussion section will compare both the electronic and the quasiparticle band structures for each of the Ni_xPt_{1-x} alloys, and these comparisons will be summarised in the Conclusions.

2. Theory

The plane-wave density functional theory (DFT) simulations presented in this work were performed using the Quantum Espresso package [18]. Both local density approximation (LDA) and generalised-gradient approximation (GGA) simulations were performed and, in both cases, spin polarisation was used with a wave-function kinetic energy cut-off of 75 Ry and a charge density/potential cut-off of 900 Ry. A Brillouin zone sampling of (20 × 20 × 20) was used together with a first-order Methfessel-Paxton smearing of 0.02 Ry throughout this work [19]. Norm-conserving pseudo-potentials [20] generated using the Perdew-Wang and the Perdew-Burke-Ernzerhof (PBE) exchange-correlation functionals were used for the LDA and GGA simulations, respectively. All energies in this work are normalised to the Fermi level E_F, i.e. $E_F = 0$ eV.

The $L1_2$ and $L1_0$ structures of the $Ni_{0.25}Pt_{0.75}$ and $Ni_{0.50}Pt_{0.50}$ ordered alloys are shown in Fig. 1 and the structural parameters are summarised in Table 1. The equilibrium lattice parameter *a* of the $L1_2$ structures were determined as the minimum of the crystal's equation of state which itself was obtained by straining the crystal i.e. changing the lattice parameter *a* and calculating the total energy of the resulting unit cell. To determine the equilibrium lattice parameters *a* and *c* of the $L1_0$ structure a similar approach was used. However, in order to determine the equation of state for this latter case the crystal was strained in *a* and then allowed to relax along the c direction using damped Beeman dynamics of the Wentzcovitch extended Lagrangian [18].

The magnetic moment per Pt and Ni atom, μ_{Pt} and μ_{Ni}, presented in Table 1 are consistent with earlier DFT studies of the Pt and Ni magnetic momenta [23, 24, 25] which have estimated values of μ_{Pt} and μ_{Ni} of $0.1-0.2/0.3\mu_B$ and $0.2-0.6\mu_B$, respectively. These studies also observed that the magnetic moment of the Ni atom is consistently larger than that of the Pt atom, and that both are sensitive to the local stoichiometry. These observations are reflected in the current study. The magnitudes of both the magnetic momenta μ_{Pt} and μ_{Ni} presented in the current work agree with values presented in the more recent DFT studies of the ordered Ni-Pt alloys [16]. This latter study thoroughly investigated the effects of both spin

https://doi.org/10.1016/j.heliyon.2018.e01000

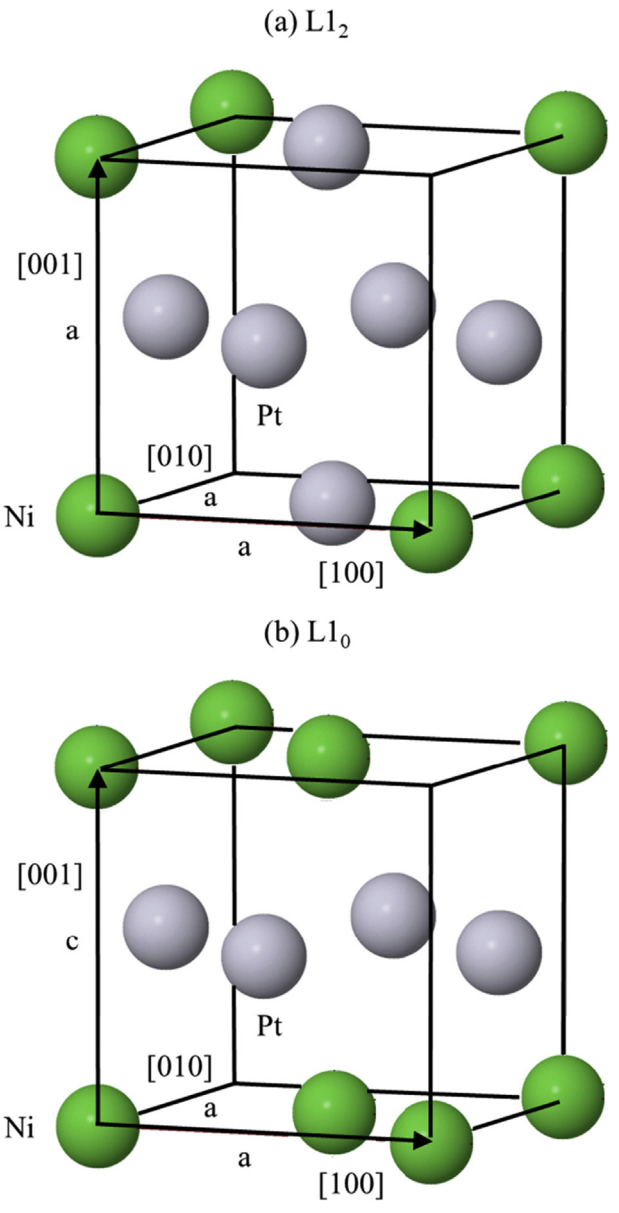

Fig. 1. The (a) $L1_2$ and (b) $L1_0$ structures of the $Ni_{0.25}Pt_{0.75}$ and $Ni_{0.50}Pt_{0.50}$ ordered alloys, respectively. The $Ni_{0.75}Pt_{0.25}$ structure is obtained by replacing each Ni (Pt) atom with a Pt (Ni) atom in the $Ni_{0.25}Pt_{0.75}$ structure.

polarisation and relativistic treatments of the ordered alloys, and the atomic origins of the moments seen in these alloys. The level of agreement between the current work and the recent work [16] suggests that the level of DFT approximation used in the current work is optimal.

Using GGA-DFT, the cohesive energy per formula unit (four atoms) E_{coh} was determined to be 19.70, 15.29 and 17.72 eV for the $Ni_{0.25}Pt_{0.75}$, $Ni_{0.75}Pt_{0.25}$ and $Ni_{0.50}Pt_{0.50}$ alloys, respectively. These values can be compared with the

https://doi.org/10.1016/j.heliyon.2018.e01000

Table 1. Summary of the structural and magnetic parameters of the for the $Ni_{0.25}Pt_{0.75}$ and $Ni_{0.75}Pt_{0.25}$ ($L1_2$) and $Ni_{0.50}Pt_{0.50}$ ($L1_0$) ordered alloys, obtained using either LDA or GGA DFT simulations performed in the current work, or experimentally in previous works. *a* and *c* are the unit cell dimensions shown in Fig. 1 and μ_{Pt} and μ_{Ni} are magnetic moment per Pt and Ni atom, respectively.

Structure		a (Å)	c (Å)	μ_{Pt} (μ_B)	μ_{Ni} (μ_B)
$Ni_{0.25}Pt_{0.75}$ ($L1_2$)	LDA	3.825	-	0.262	1.043
	GGA	3.919	-	0.348	1.284
	Exptl.	3.836[21]	-	-	-
$Ni_{0.75}Pt_{0.25}$ ($L1_2$)	LDA	3.604	-	0.384	0.973
	GGA	3.752	-	0.177	1.198
	Exptl.	3.645[21]	-	-	-
$Ni_{0.50}Pt_{0.50}$ ($L1_0$)	LDA	3.812	3.539	0.418	1.044
	GGA	3.922	3.644	0.397	1.243
	Exptl.	3.814[21]	3.533[22]	-	-

experimental values of the cohesive energy of $E_{coh}(Ni_4) = 17.76$ eV and $E_{coh}(Pt_4) = 23.36$ eV [26]. The calculated alloys cohesive energies are therefore within 5−10% of the weighted average of the pure elements, which is similar to the level of agreement seen in previous computational estimates of $E_{coh}(Ni_{0.25}Pt_{0.75})$ [27].

To estimate accurately the band structure of the ordered Ni_xPt_{1-x} phases, and to evaluate the error in calculations of the band structures which use GGA/LDA approximation, the quasiparticle energies were calculated within the GW approximation for the self-energy using the YAMBO package [28]. This problem has been comparatively widely investigated for semiconductor systems [29, 30] compared to the more limited studies of metallic systems [31]. In the current work, for each band structure a single-shot G_0W_0 calculation [32] with RPA (real axis integration) was conducted. For the $Ni_{0.25}Pt_{0.75}$, $Ni_{0.75}Pt_{0.25}$ and $Ni_{0.50}Pt_{0.50}$ ordered alloys the Drude plasmon peaks were determined by extrapolation [33] to be 7.74, 11.09 and 9.415 eV, respectively.

In order to quantify the differences in the curvature of the quasiparticle and DFT band structures, the normalised gradient difference R_k^{qp} of the quasi-particle and GGA-corrected bare electron dispersions was defined as

$$R_k^{qp}(E_{bare}) = 2 \times \frac{\left|\left(\frac{dE_{qp}}{dk}\right)\right| - \left|\left(\frac{dE_{bare}}{dk}\right)\right|}{\left|\left(\frac{dE_{qp}}{dk}\right)\right| + \left|\left(\frac{dE_{bare}}{dk}\right)\right|} \quad (1)$$

E_{qp} and E_{bare} are the energies of the quasi-particle and GGA-corrected bare electron dispersions, respectively. Similarly, the normalised gradient difference R_k^{bare} of the LDA- and GGA-corrected bare electron dispersions was defined as

https://doi.org/10.1016/j.heliyon.2018.e01000

$$R_k^{bare}(E_{bare}) = 2 \times \frac{\left|\left(\frac{dE_{bare}^{LDA}}{dk}\right)\right| - \left|\left(\frac{dE_{bare}}{dk}\right)\right|}{\left|\left(\frac{dE_{bare}^{LDA}}{dk}\right)\right| + \left|\left(\frac{dE_{bare}}{dk}\right)\right|} \quad (2)$$

$E_{bare}^{LDA}$is the energy of the LDA-corrected bare electron dispersion. The resulting histogram of both R_k^{qp} is denoted N_{Tot}.

The differences in the energies of the band structures determined by the quasiparticle and DFT approaches can be seen by comparing the quasiparticle and DFT energies, which are denoted E_{qp} and E_{bare} respectively. In the current work, this comparison is only performed between quasiparticle energies and DFT energies obtained using the GGA approximation. The linearity of the relationship between E_{qp} and E_{bare} provides a quantification of the quasiparticle weight [34] which itself is a function of the gradient of the self-energy of the quasiparticle with energy. The linear component of the curve of E_{qp}versus E_{bare} was extracted using the linear curve defined in Eq. (3)

$$E_{qp;LF} = mE_{bare} + c \quad (3)$$

Both conventional and robust fitting [35] were used to extract m and c. No significant differences were seen between the two methods though the results presented in the current work were obtained from robust fitting.

The non-linear residual component of the E_{qp}versus E_{bare} curve was defined using Eq. (4)

$$E_{qp;Resid} = E_{qp} - E_{qp;LF} \quad (4)$$

$E_{qp;Resid}$ can be used to quantify the linearity of the curve of E_{qp}versus E_{bare} using Eq. (5)

$$\chi^2_{Resid} = \sum_{i=1}^{N} \frac{{E_{qp;Resid}}^2}{N} \quad (5)$$

N is the number of energies at a particular k-point.

The non-linear residual$E_{qp;Resid}$ was modelled using a sequence of functions

$$E_{qp;Resid}^{d;linear} = c_1 + c_2 S_{Pt\ d} + c_3 S_{Ni\ d} \quad (6)$$

$$E_{qp;Resid}^{sd;linear} = c_1 + c_2 S_{Pt\ s} + c_3 S_{Pt\ d} + c_4 S_{Ni\ s} + c_5 S_{Ni\ d} \quad (7)$$

$$E_{qp;Resid}^{d;quad} = c_1 + c_2 S_{Pt\ d} + c_3 S_{Pt\ d}^2 + c_4 S_{Ni\ d} + c_5 S_{Ni\ d}^2 \quad (8)$$

https://doi.org/10.1016/j.heliyon.2018.e01000

$$E^{sd}_{qp;Resid} = c_1 + c_2 S_{Pt\ s} + c_3 S_{Pt\ d} + c_4 S^2_{Pt\ d} + c_5 S_{Ni\ s} + c_6 S_{Ni\ d} + c_7 S^2_{Ni\ d} \quad (9)$$

$S_{Pt\ s}$, $S_{Ni\ s}$, $S_{Pt\ d}$ and $S_{Ni\ d}$are the sum of the Pt and Ni s and d wave-function coefficients, respectively. During this fitting process the constant term c_1 could absorbed into the constant term c used in Eq. (1) with no significant increase to the best-fit value of χ^2_{Resid}. The overall quality of fit was

$$\chi^2_{Fit} = \sum_{i=1}^{N} \frac{\left(E_{qp;Resid} - E_{qp;Fit}\right)^2}{N} \quad (10)$$

In Eq. (10) $E_{qp;Fit}$ was one of either $E^{d;linear}_{qp;Resid}$, $E^{sd;linear}_{qp;Resid}$, $E^{d;quad}_{qp;Resid}$or $E^{sd}_{qp;Resid}$.

3. Results & discussion

Fig. 2 shows the band structures for the $Ni_{0.25}Pt_{0.75}$, $Ni_{0.75}Pt_{0.25}$ and $Ni_{0.50}Pt_{0.50}$ ordered alloys calculated within both the DFT and quasiparticle approximations. Only the spin-up band structures are presented in the current work, for brevity. The latter band structures are presented close the Γ point compared to the DFT band structures as the comparative discussion of these two approaches will focus on differences at the Γ point. Each DFT band structure contains a low-lying s-like feature, which has energy of approximately -10 eV at the Γ point. This feature remains separated from the higher energy d-band at low values of k, where k is the distance in reciprocal space to the Γ point. This separation becomes less at larger values of k, for example at the R k-point and in the R-A regions of the $L1_2$ and $L1_0$ lattices, respectively. The assignment of orbital character to a particular band and at a particular energy is based on the band structures presented in supplementary Fig. S1, which shows the projection of the crystal wave-function onto the s and d spin-polarised atomic wave-functions. These projections are shown as partial density of states (PDOS) in supplementary Fig. S2.

At higher energies, the occupied bands of the DFT band structures have significant d character and contain flat, linear (non-dispersive) regions at approximately -3 eV at the Γ point. The observation of non-dispersive regions is a key observation in the DFT band structures. If these structures are compared with the quasiparticle band structures, the dispersion is seen to increase within these non-dispersive regions and elsewhere within the band-structures. This means that GW approximation predicts that the quasiparticles mobility can be greater that of the bare electron. This prediction removes the unusual flat regions from the dispersion.

Quantitatively, changes in the curvature are analysed using a simple numerical metric $R^{qp}_k(E_{bare})$ which was defined in Eq. (1). The metric shows the fractional change in the curvature of the band structure when the quasiparticle approximation is applied. Fig. 3 shows histograms of this parameter at the Γ point of the spin-up

https://doi.org/10.1016/j.heliyon.2018.e01000

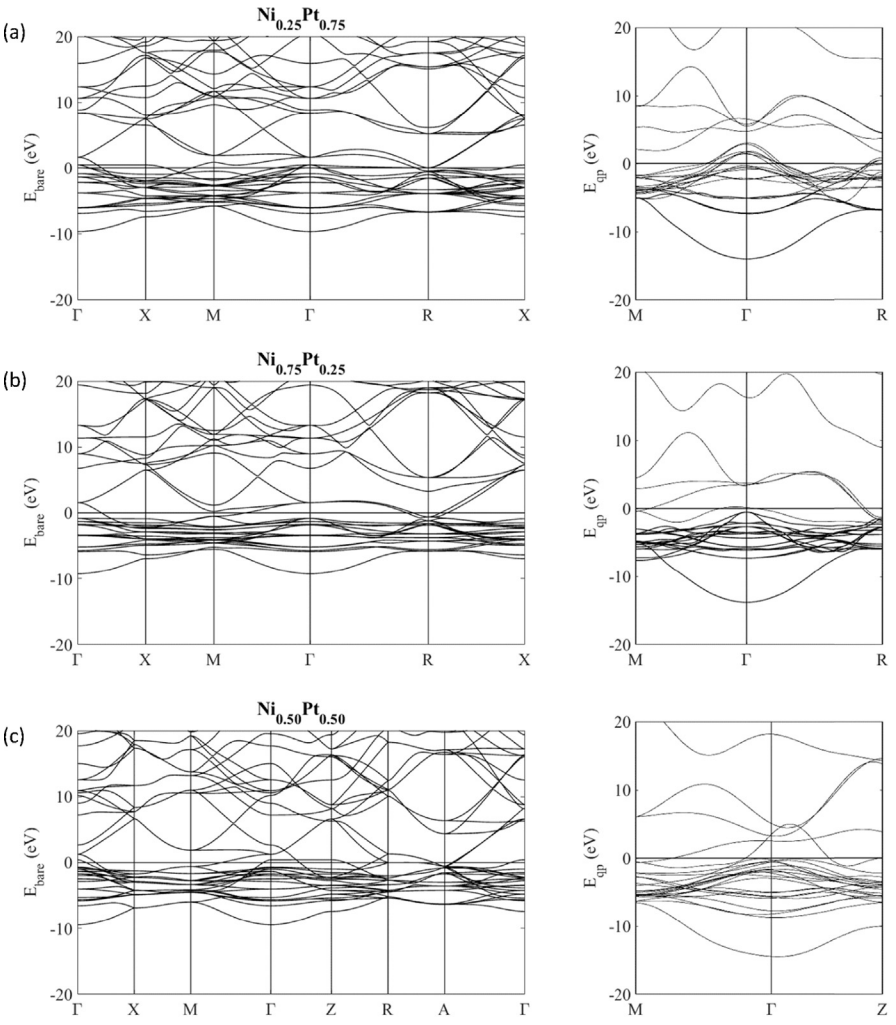

Fig. 2. Band structures for the (a) $Ni_{0.25}Pt_{0.75}$, (b) $Ni_{0.75}Pt_{0.25}$ and (c) $Ni_{0.50}Pt_{0.50}$ ordered alloys, obtained using both the DFT (E_{bare}) and quasiparticle (E_{qp}) approximations.

band structures for each of the $Ni_{0.25}Pt_{0.75}$, $Ni_{0.75}Pt_{0.25}$ and $Ni_{0.50}Pt_{0.50}$ ordered alloys. The histograms show that the curvature generally increases as the quasiparticle approximation is applied, as the average $R_k^{qp}(E_{bare}) > 0$. A similar set of histograms was obtained for the spin-down band structures at the same k-point for each of the ordered alloys.

Table 2 summarises the extension of this analysis across all of the high symmetry k-points for each of the ordered alloys. Comparing $R_k^{qp}(E_{bare})$ at the Γ, X and M points for each alloy shows that the increased curvature is largest at the Γ point independent of the alloys structure, and that the $R_k^{qp}(E_{bare})$generally decreases as distance from the Γ point increases. This latter conclusion can be confirmed quantitatively by considering the distances from the Γ point to the X and M points summarised in Table 3. A similar behaviour is apparent when considering the out-of-plane k-points

https://doi.org/10.1016/j.heliyon.2018.e01000

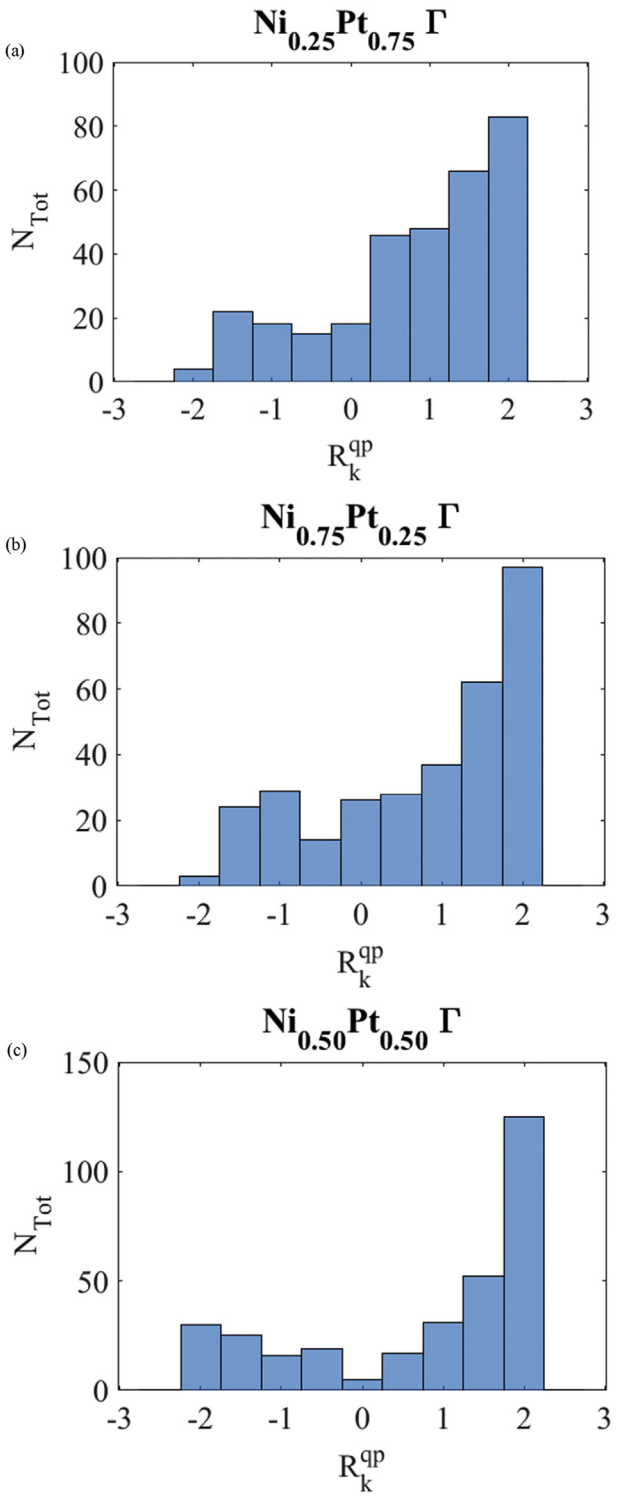

Fig. 3. Histograms of the normalised gradient difference R_k^{qp} of the quasiparticle and GGA-corrected bare electron dispersions, evaluated at the Γ point for the (a) $Ni_{0.25}Pt_{0.75}$, (b) $Ni_{0.75}Pt_{0.25}$ and (c) $Ni_{0.50}Pt_{0.50}$ ordered alloys.

https://doi.org/10.1016/j.heliyon.2018.e01000

Table 2. Summary of the average normalised gradient differences $\langle R_k^{qp}(E_{bare})\rangle$ and $\langle R_k^{bare}(E_{bare})\rangle$ for the $Ni_{0.25}Pt_{0.75}$ and $Ni_{0.75}Pt_{0.25}$ ($L1_2$) and $Ni_{0.50}Pt_{0.50}$ ($L1_0$) ordered alloys, evaluated at the high-symmetry Γ, X, M and R reciprocal space positions for the $L1_2$ alloys, and at the Γ, X, M, Z, R and A positions for the $L1_0$ alloy.

Structure	Average gradient difference	Γ	X	M	Z	R	A
$Ni_{0.25}Pt_{0.75}$ ($L1_2$)	$\langle R_k^{qp}(E_{bare})\rangle$	0.804	0.456	0.340	-	0.330	-
	$\langle R_k^{bare}(E_{bare})\rangle$	−0.066	0.057	0.145	-	−0.053	-
$Ni_{0.50}Pt_{0.50}$ ($L1_0$)	$\langle R_k^{qp}(E_{bare})\rangle$	0.755	0.519	0.373	0.056	0.300	0.246
	$\langle R_k^{bare}(E_{bare})\rangle$	0.070	0.004	0.101	−0.019	0.038	−0.007
$Ni_{0.75}Pt_{0.25}$ ($L1_2$)	$\langle R_k^{qp}(E_{bare})\rangle$	0.786	0.592	0.482	-	0.513	-
	$\langle R_k^{bare}(E_{bare})\rangle$	0.165	0.167	0.201	-	0.326	-

Table 3. Summary of the k-space distances between the Γ point and each of the remaining high-symmetry points. Units are of these distances are $2\pi/a$, where a is the length defined in Fig. 1. The out-of-plane length c for the $L1_0$ $Ni_{0.50}Pt_{0.50}$ structure was 0.9292, and was deduced from the parameters presented in Table 1.

Structure	X	M	Z	R	A
$L1_2$	0.500	0.707	-	0.866	-
$L1_0$	0.500	0.707	0.464	0.682	0.846

Z, R and A and shows that the quasiparticle corrections are most significant at the Γ point.

To compare the importance of the quasiparticle correction with the choice of exchange-correlation functional, the metric $R_k^{bare}(E_{bare})$ was defined in Eq. (2). This metric shows the fractional differences in the curvature of the band structure when either the GGA or the LDA approximation was used. The k-resolved average values of this parameter are summarised in Table 2 and shows that the importance of exchange-correlation functional is less than that of the quasiparticle approximation as $R_k^{qp}(E_{bare}) > R_k^{bare}(E_{bare})$for all k-points.

Fig. 4 shows the quasiparticle energy E_{qp} versus DFT energy E_{bare} evaluated at the Γ point for each of the ordered $Ni_{0.25}Pt_{0.75}$, $Ni_{0.75}Pt_{0.25}$ and $Ni_{0.50}Pt_{0.50}$ alloys. The simplest approximation of these curves − i.e. the simplest model for the quasiparticle correction - was determined by fitting the linear model $E_{qp;LF}$to the curve. Though this simple model reproduces the general increase of E_{qp} with E_{bare} the it is clear in Fig. 4 that the model has insufficient complexity to perfectly model the dependence of E_{qp} on E_{bare}. This discrepancy is quantified by the quality of fit $\chi^2_{Resid}$of the linear model. χ^2_{Resid} is shown in Fig. 5 for each of the high symmetry k-points. To highlight the k-dependence of $\chi^2_{Resid}$the abscissa of Fig. 5 is k, whose

https://doi.org/10.1016/j.heliyon.2018.e01000

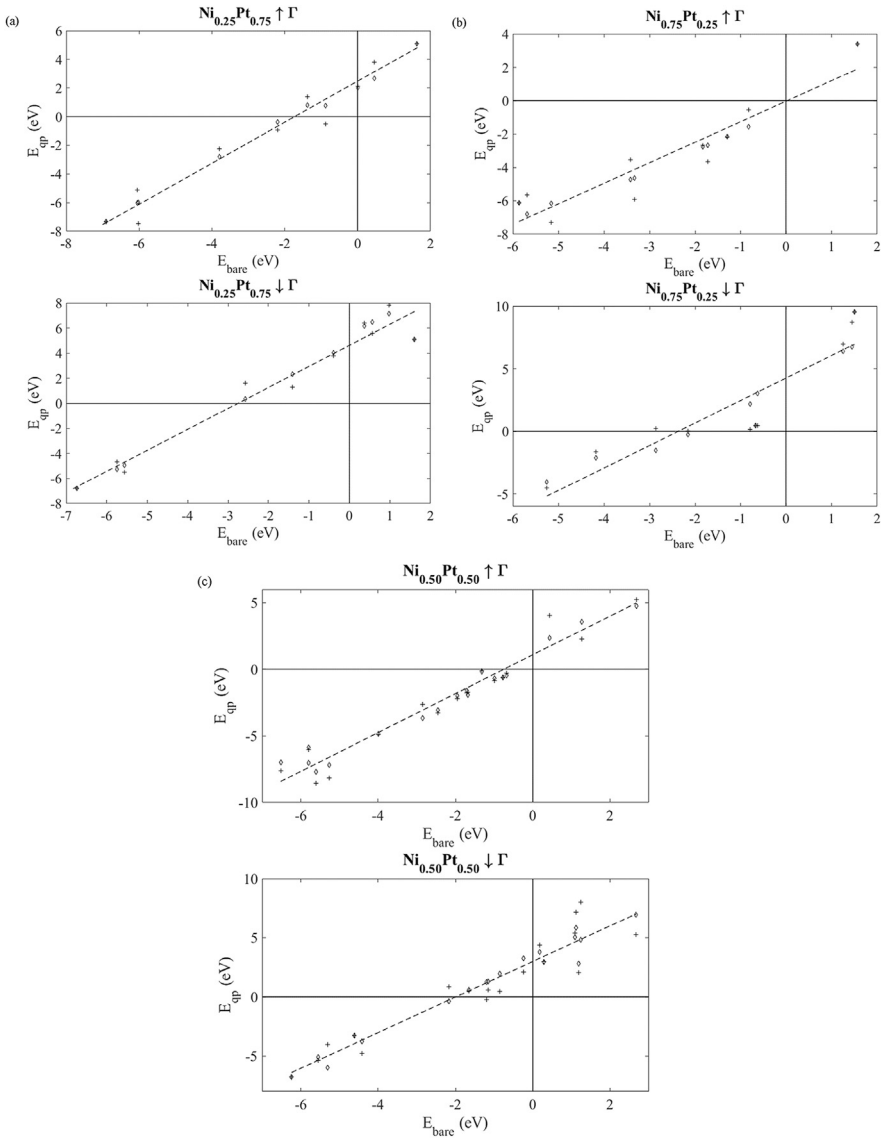

Fig. 4. Quasiparticle energy E_{qp} versus DFT energy E_{bare} for the (a) $Ni_{0.25}Pt_{0.75}$, (b) $Ni_{0.75}Pt_{0.25}$ and (c) $Ni_{0.50}Pt_{0.50}$ ordered alloys. The energies were evaluated at the Γ point and the up/down arrows in the title of each panel denote the spin/down energies, respectively. The addition signs ('+') denote the E_{qp} and E_{bare} energies obtained directly from the quasiparticle and DFT simulations. The linear dashed lines were obtained by fitting Eq. (3) to the E_{qp} and E_{bare} energies obtained from the GW and DFT simulations, and the diamond symbols were obtained by fitting Eq. (9) to the residual (see text).

value can be converted into k-point by comparison with the distances in Table 3. The general increase in χ^2_{Resid} with k demonstrates that the quasiparticle correction becomes increasingly non-linear as the distance from the Γ point increases. This dependence is in counterpoint to the increases in curvature seen at the Γ point and discussed earlier. This indicates that the quasiparticle weight is greater and that the quasiparticle correction is increasingly linear at low values of k.

https://doi.org/10.1016/j.heliyon.2018.e01000

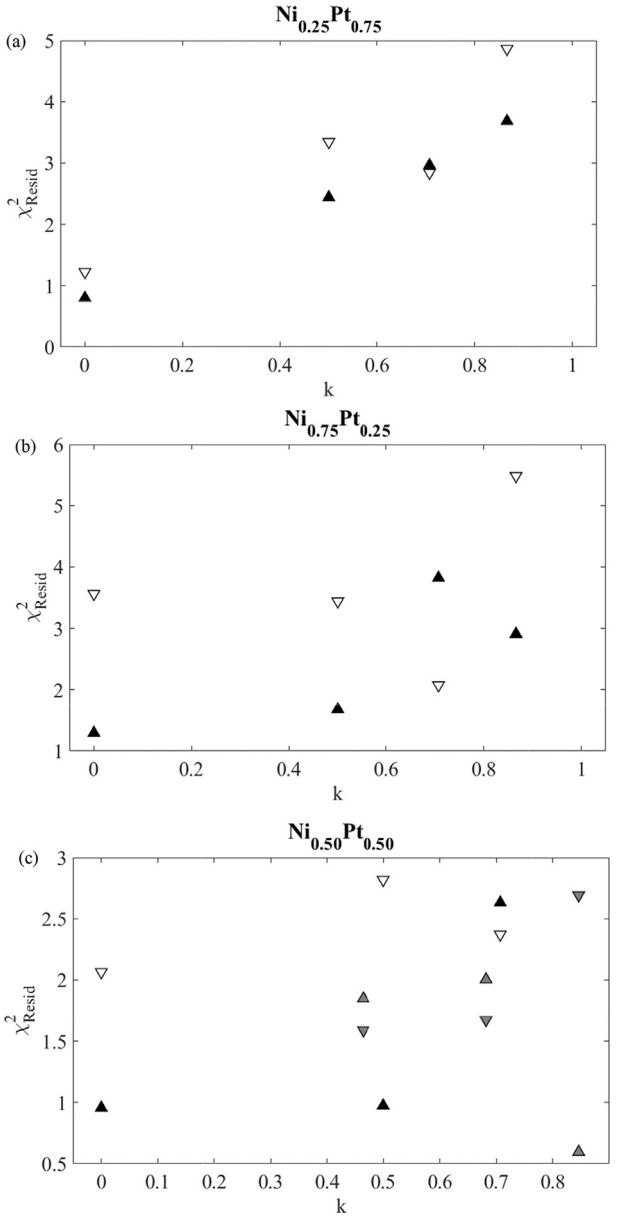

Fig. 5. Residual quality-of-fit parameter χ^2_{Resid} for the (a) $Ni_{0.25}Pt_{0.75}$, (b) $Ni_{0.75}Pt_{0.25}$ and (c) $Ni_{0.50}Pt_{0.50}$ ordered alloys, evaluated at the high-symmetry Γ, X, M and R ($L1_2$) and the Γ, X, M, Z, R and A ($L1_0$) positions in reciprocal-space. The filled triangles (empty inverted triangles) were obtained during regression analysis of the spin up (down) DFT and GW energies. The k distances are those between the high-symmetry reciprocal-space point and the Γ point, and shown in Table 3.

https://doi.org/10.1016/j.heliyon.2018.e01000

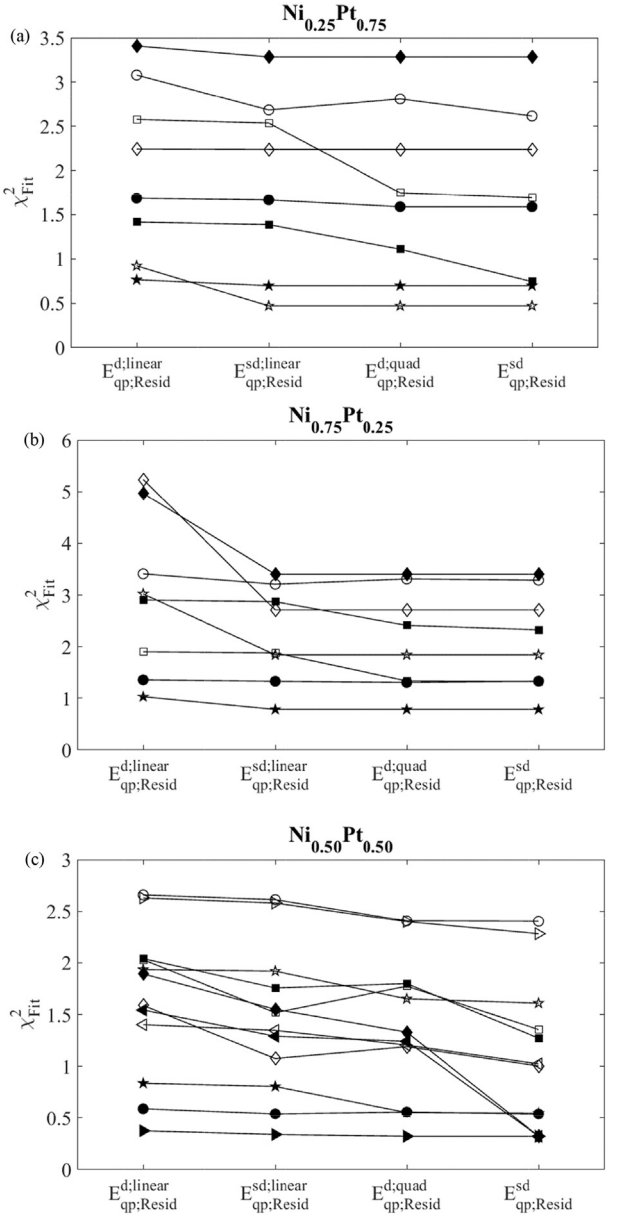

Fig. 6. Quality-of-fit parameter χ^2_{Fit} for the non-linear residual models defined in Eqs. (6), (7), (8), and (9). Each model was applied to the (a) $Ni_{0.25}Pt_{0.75}$, (b) $Ni_{0.75}Pt_{0.25}$ ($L1_2$) and (c) $Ni_{0.50}Pt_{0.50}$ ($L1_0$) ordered alloys and evaluated at the high-symmetry Γ (pentagrams), X (circles), M (squares) and R (diamonds) reciprocal space positions for the $L1_2$ alloys, and at the Γ (pentagrams), X (circles), M (squares), Z (left-pointed triangles), R (diamonds) and A (right-pointed triangles) positions for the $L1_0$ alloy. The clear (filled) markers denote fitting to the spin up (down) case. The abscissa coordinate shows the non-linear model.

https://doi.org/10.1016/j.heliyon.2018.e01000

The residual component $E_{qp;Resid}$ was modelled using one of either of $E^{d;linear}_{qp;Resid}$, $E^{sd;linear}_{qp;Resid}$, $E^{d;quad}_{qp;Resid}$or $E^{sd}_{qp;Resid}$ which were defined in Eqs. (6), (7), (8), and (9). The quality of fit $\chi^2_{Fit}$for each function is shown in Fig. 6 and the actual values of E_{qp} obtained after fitting $E^{sd}_{qp;Resid}$, the highest level model, are shown on Fig. 4. By comparing the values of χ^2_{Fit} obtained using $E^{d;linear}_{qp;Resid}$and $E^{sd;linear}_{qp;Resid}$it is clear that the quasiparticle correction requires the inclusion of s states or of non-linear d terms. This initial observation is contrary to the usual treatment of transition metal alloys which ignores s states. Fig. 6 also shows that χ^2_{Fit}converges rapidly with the level of model used. Consequently, to improve the quality of fit to $E_{qp;Resid}$a significant number of higher order terms in both s and d states are required. However as the total number of terms in the $\chi^2_{Resid}$is equal to the number of E_{qp} and E_{bare} energy pairs, i.e. the number of states at each k-point of each band structure in Fig. 2, the analysis was truncated at $E^{sd}_{qp;Resid}$before it became unstable. This instability would arise because the number of unknowns becomes close to the number of E_{qp} and E_{bare} energy pairs [35].

4. Conclusions

The current work has investigated the electronic and quasiparticle band structures for the ordered $L1_2$ phases of Ni_xPt_{1-x} ($x = 0.25$ and 0.75) and the ordered $L1_0$ phase of $Ni_{0.50}Pt_{0.50}$. These investigations have been performed using the Quantum Espresso package to perform density functional theory calculations of the electronic band structures and the YAMBO package to calculate the quasiparticle corrections. For each ordered phase, the quasiparticle correction generally separated the states in energy and was seen to increase the curvature of the band structure. These increases were notable around the Γ point where non-dispersive bands − that is, bands which appear flat in the electronic band structure − were shown to be dispersive under the quasiparticle correction.

Quantitatively, changes in the curvature have been analysed using a simple numerical metric $R^{qp}_k(E_{bare})$. Using this metric is has been seen that the curvature changes decrease with distance from the Γ point indicating that the quasiparticle effects are strongest close to the Γ point. The comparative metric $R^{bare}_k(E_{bare})$ has shown that the quasiparticle correction is numerically more significant than the choice of exchange-correlation functional in determining the alloy band structure. Simple linear modelling of the quasiparticle correction has been shown to reproduce the general trends of the quasiparticle correction. However, non-linear modelling of the correction has been shown to rapidly converge with the inclusion of P and Ni s and d states or of non-linear d states, and would require a significant number of higher order terms to more accurately describe the correction. The limitations of this approach are discussed.

https://doi.org/10.1016/j.heliyon.2018.e01000

Declarations

Author contribution statement

Ian Shuttleworth: Conceived and designed the analysis; Analyzed and interpreted the data; Contributed analysis tools or data; Wrote the paper.

Funding statement

This research did not receive any specific grant from funding agencies in the public, commercial, or not-for-profit sectors.

Competing interest statement

The authors declare no conflict of interest.

Additional information

Supplementary content related to this article has been published online at https://doi.org/10.1016/j.heliyon.2018.e01000.

References

[1] M.C. Cadeville, J.L. Morán-López, Magnetism and spatial order in transition metal alloys, Phys. Rep. 153 (6) (1987) 331−399.

[2] M.C. Cadeville, C.E. Dahmani, F. Kern, Magnetism and spatial order in Ni-Pt and Co-Pt alloys, J. Magn. Magn Mater. 54−57 (1986) 1055−1066.

[3] C.E. Dahmani, M.C. Cadeville, J.M. Sanchez, J.L. Morán-López, Ni-Pt phase diagram : experiment and theory, Phys. Rev. Lett. 55 (11) (1985) 1208−1211.

[4] J. Staunton, P. Weinberger, B.L. Gyorffy, On the electronic structure of paramagnetic Ni_cPt_{1-c} alloys: a relativistic calculation, J. Phys. F Met. Phys. 13 (1983) 779−798.

[5] N.J. Shevchik, D. Bloch, XPS d bands and core levels of Pt-Ni alloys, J. Phys. F Met. Phys. 7 (3) (1977) 543−550.

[6] F.J. Pinski, B. Ginatempo, D.D. Johnson, J.B. Staunton, G.M. Stocks, B.L. Gyorffy, Origins of compositional order in NiPt alloys, Phys. Rev. Lett. 66 (1991) 766−769.

[7] P.P. Singh, A. Gonis, P.E.A. Turchi, Toward a unified approach to the study of metallic alloys: application to the phase stability of Ni-Pt, Phys. Rev. Lett. 71 (10) (1993) 1605−1608.

[8] A. Marmodoro, J.B. Staunton, Disorder in materials with complex crystal structures: the non-local coherent potential approximation for compounds with multiple sublattices, J. Phys. Conf. Ser. 286 (2011) 012033.

[9] T.-U. Nahm, J.-Y. Kim, S.-J. Oh, S.-M. Chung, J.-H. Park, J.W. Allen, K. Jeong, S. Kim, Photoemission study of electronic structures of disordered Ni-Pt and Cu-Pt alloys, Phys. Rev. B Condens. Matter 54 (11) (1996) 7807−7815.

[10] T.-U. Nahm, H.-J. Noh, J.-Y. Kim, S.-J. Oh, Electron spectroscopic evidence of electron correlation in Ni-Pt alloys: comparison with specific heat measurement, J. Phys. Condens. Matter 15 (2003) 3191−3202.

[11] V.R. Stamenkovic, B. Fowler, B.S. Mun, G. Wang, P.N. Ross, C.A. Lucas, N.M. Marković, Improved oxygen reduction activity on $Pt_3Ni(111)$ via increased surface site availability, Science 315 (2007) 493−497.

[12] V.R. Stamenkovic, B.S. Mun, M. Arenz, K.J.J. Mayrhofer, C.A. Lucas, G. Wang, P.N. Ross, N.M. Marković, Trends in electrocatalysis on extended and nanoscale Pt bimetallic alloy surfaces, Nat. Mater. 6 (3) (2007) 241−247.

[13] M. Polak, L. Rubinovich, The interplay of surface segregation and atomic order in alloys, Surf. Sci. Rep. 38 (2000) 127−194.

[14] I.G. Shuttleworth, Binding site transitions across strained oxygenated and hydroxylated Pt(111), ChemistryOpen 7 (2018) 356−369.

[15] I.G. Shuttleworth, Strain engineering of H/transition metal systems, Surf. Sci. 661 (2017) 49−59.

[16] I.G. Shuttleworth, The effects of strain on the ordered phases of Ni_xPt_{1-x} (x = 0.25, 0.5, and 0.75), Chem. Phys. Lett. 689 (2017) 41−47.

[17] I.G. Shuttleworth, Magnetism in the strained ordered phases of Pt_xFe_{1-x} and Pt_xCo_{1-x} (x=0.25, 0.5, and 0.75), J. Phys. Chem. Solid. 114 (2018) 153−162.

[18] P. Giannozzi, O. Andreussi, T. Brumme, O. Bunau, M. Buongiorno Nardelli, M. Calandra, R. Car, C. Cavazzoni, D. Ceresoli, M. Cococcioni, N. Colonna, I. Carnimeo, A. Dal Corso, S. de Gironcoli, P. Delugas, R.A. DiStasio Jr., A. Ferretti, A. Floris, G. Fratesi, G. Fugallo, R. Gebauer, U. Gerstmann, F. Giustino, T. Gorni, J. Jia, M. Kawamura, H.-Y. Ko, A. Kokalj, E. Küçükbenli, M. Lazzeri, M. Marsili, N. Marzari, F. Mauri, N.L. Nguyen, H.-V. Nguyen, A. Otero-de-la-Roza, L. Paulatto, S. Poncé, D. Rocca, R. Sabatini, B. Santra, M. Schlipf, A.P. Seitsonen, A. Smogunov, I. Timrov, T. Thonhauser, P. Umari, N. Vast, X. Wu, S. Baroni, Advanced capabilities for materials modelling with Quantum ESPRESSO, J. Phys. Condens. Matter 29 (2017) 465901.

 https://doi.org/10.1016/j.heliyon.2018.e01000

[19] M. Methfessel, A.T. Paxton, High-precision sampling for Brillouin-zone integration in metals, Phys. Rev. B Condens. Matter 40 (1989) 3616−3621.

[20] The x.pbe-mt_fhi.UPF and x.pw-mt_fhi.UPF (x=Ni or Pt) pseudopotentials were used for the GGA and LDA simulations, respectively, from the Quantum ESPRESSO pseudopotential data base: http://www.quantum-espresso.org/pseudopotentials.

[21] A. Pisanty, C. Amador, Y. Ruiz, M. de la Vega, Band structures of Ni_3Pt and $NiPt_3$, Z. Phys. B Condens. Matter 80 (1990) 237−239.

[22] W.B. Pearson, A Handbook of Lattice Spacings and Structures of Metals and Alloys, Pergamon Press, Oxford, 1967.

[23] U. Kumar, P.K. Mukhopadhyay, B. Sanyal, O. Eriksson, P. Nordblad, D. Paudyal, K. Tarafder, A. Mookerjee, Experimental and theoretical study of annealed Ni-Pt alloys, Phys. Rev. B Condens. Matter 74 (6) (2006) 064401.

[24] P.P. Singh, Relativity and magnetism in Ni-Pd and Ni-Pt alloys, J. Magn. Magn Mater. 261 (2003) 347−352.

[25] D. Paudyal, T. Saha-Dasgupta, A. Mookerjee, Magnetic properties of X-Pt (X=Fe, Co, Ni) alloy systems, J. Phys. Condens. Matter 16 (2004) 2317−2334.

[26] C. Kittel, Einführung in die Festkörperphysik, R. Oldenbourg Verlag, München, 1991.

[27] T. Jacob, W.A. Goddard III, Adsorption of atomic H and O on the (111) surface of Pt_3Ni alloys, J. Phys. Chem. B 108 (2004) 8311−8323.

[28] A. Marini, C. Hogan, M. Grüning, D. Varsano, yambo: an ab initio tool for excited state calculations, Comput. Phys. Commun. 180 (2009) 1392−1403.

[29] L.J. Sham, M. Schlüter, Density-functional theory of the energy gap, Phys. Rev. Lett. 51 (1983) 1888−1891.

[30] J.P. Perdew, M. Levy, Physical content of the exact Kohn-Sham orbital energies: band gaps and derivative discontinuities, Phys. Rev. Lett. 51 (1983) 1884−1887.

[31] A. Marini, G. Onida, R. Del Sole, Quasiparticle electronic structure of copper in the GW approximation, Phys. Rev. Lett. 88 (1) (2002) 016403.

[32] L. Hedin, New method for calculating the one-particle Green's function with application to the electron-gas problem, Phys. Rev. 139 (1965) A796−A823.

https://doi.org/10.1016/j.heliyon.2018.e01000

[33] L.S. Abdallah, T.M. Tawalbeh, I.V. Vasiliev, S. Zollner, C. Lavoie, A. Ozcan, M. Raymond, Optical conductivity of $Ni_{1-x}Pt_x$ alloys ($0<x<0.25$) from 0.76 to 6.6 eV, AIP Adv. 4 (2014) 017102.

[34] W.G. Aulbur, L. Jönsson, J.W. Wilkins, Quasiparticle calculations in solids, Solid State Phys. 54 (2000) 1−218.

[35] W.H. Press, B.P. Flannery, S.A. Teukolsky, W.T. Vetterling, Numerical Recipes in C, Cambridge University Press, 2002.

https://doi.org/10.1016/j.heliyon.2018.e01000